Toxicology 440 (2020) 152478

Contents lists available at ScienceDirect

Toxicology

journal homepage: www.elsevier.com/locate/toxicol

Dual mechanisms suppress meloxicam bioactivation relative to sudoxicam

Dustyn A. Barnette[a], Mary A. Schleiff[a], Laura R. Osborn[a,1], Noah Flynn[b], Matthew Matlock[b], S. Joshua Swamidass[b], Grover P. Miller[a,*]

[a] Department of Biochemistry and Molecular Biology, University of Arkansas for Medical Sciences, 4301 W Markham St, Little Rock, AR, 72205, United States
[b] Department of Pathology and Immunology, 660 S Euclid Ave, Washington University, St. Louis, MO, 63130, United States

ARTICLE INFO

Keywords:
Meloxicam
Sudoxicam
Thiazole
Bioactivation
Liver toxicity
Kinetics

ABSTRACT

Thiazoles are biologically active aromatic heterocyclic rings occurring frequently in natural products and drugs. These molecules undergo typically harmless elimination; however, a hepatotoxic response can occur due to multistep bioactivation of the thiazole to generate a reactive thioamide. A basis for those differences in outcomes remains unknown. A textbook example is the high hepatotoxicity observed for sudoxicam in contrast to the relative safe use and marketability of meloxicam, which differs in structure from sudoxicam by the addition of a single methyl group. Both drugs undergo bioactivation, but meloxicam exhibits an additional detoxification pathway due to hydroxylation of the methyl group. We hypothesized that thiazole bioactivation efficiency is similar between sudoxicam and meloxicam due to the methyl group being a weak electron donator, and thus, the relevance of bioactivation depends on the competing detoxification pathway. For a rapid analysis, we modeled epoxidation of sudoxicam derivatives to investigate the impact of substituents on thiazole bioactivation. As expected, electron donating groups increased the likelihood for epoxidation with a minimal effect for the methyl group, but model predictions did not extrapolate well among all types of substituents. Through analytical methods, we measured steady-state kinetics for metabolic bioactivation of sudoxicam and meloxicam by human liver microsomes. Sudoxicam bioactivation was 6-fold more efficient than that for meloxicam, yet meloxicam showed a 6-fold higher efficiency of detoxification than bioactivation. Overall, sudoxicam bioactivation was 15-fold more likely than meloxicam considering all metabolic clearance pathways. Kinetic differences likely arise from different enzymes catalyzing respective metabolic pathways based on phenotyping studies. Rather than simply providing an alternative detoxification pathway, the meloxicam methyl group suppressed the bioactivation reaction. These findings indicate the impact of thiazole substituents on bioactivation is more complex than previously thought and likely contributes to the unpredictability of their toxic potential.

1. Introduction

Thiazoles impart critical biological activities for a wide range of natural molecules (Ayati et al., 2015) and based on that precedent, this substructure serves as a "privileged scaffold (Kumar et al., 2016)" in the design of effective therapeutics. Nevertheless, those applications may also pose risks of toxicity for patients due to that same presence of a thiazole. This substructure is an aromatic heterocyclic five-membered ring containing sulfur and nitrogen at positions 1 and 3, whose structure is considered to be the most metabolically stable five-membered heterocycle (Smith, 2011). Many thiazole-containing drugs on the market have little to no toxicity associated with them ("LiverTox", 2018) including the anticoagulant edoxaban (Liakoni et al., 2015), the antibiotic ceftazidime (GlaxoSmithKline, 2007), the anticancer agent dasatinib (Sasaki et al., 2016), and the antiulcer nazitidine (Reliant, 2004). Unlike those cases, the use of thiazoles in other drugs has led to severe associated toxicities in the clinic. The antifungal agent ravuconazole was discontinued in 2007 (Ayati et al., 2015), and the previously widely used antimicrobial sulfathiazole is now rarely prescribed in favor of newer, less toxic alternatives ("Sulfathiazole", 2018). The commonly used topical antifungal thiabendazole can cause severe kidney damage when taken orally (Mizutani et al., 1994a). Knowledge of these examples and others underlies the classification of the thiazole as a "structural alert" for the possibility of toxicity, yet the probability remains unknown and hence unpredictable.

Identifying drugs susceptible to toxicity requires an understanding of the mechanism(s) driving that potential. Thiazole toxicity likely involves an initial oxidation event catalyzed by cytochrome P450

* Corresponding author.
E-mail address: millergroverp@uams.edu (G.P. Miller).
[1] Present address: Department of Chemistry and Physics, Ave Maria University, 5050 Ave Maria Blvd, Ave Maria, FL, 34142, United States.

https://doi.org/10.1016/j.tox.2020.152478
Received 22 February 2020; Received in revised form 17 April 2020; Accepted 24 April 2020
Available online 11 May 2020
0300-483X/

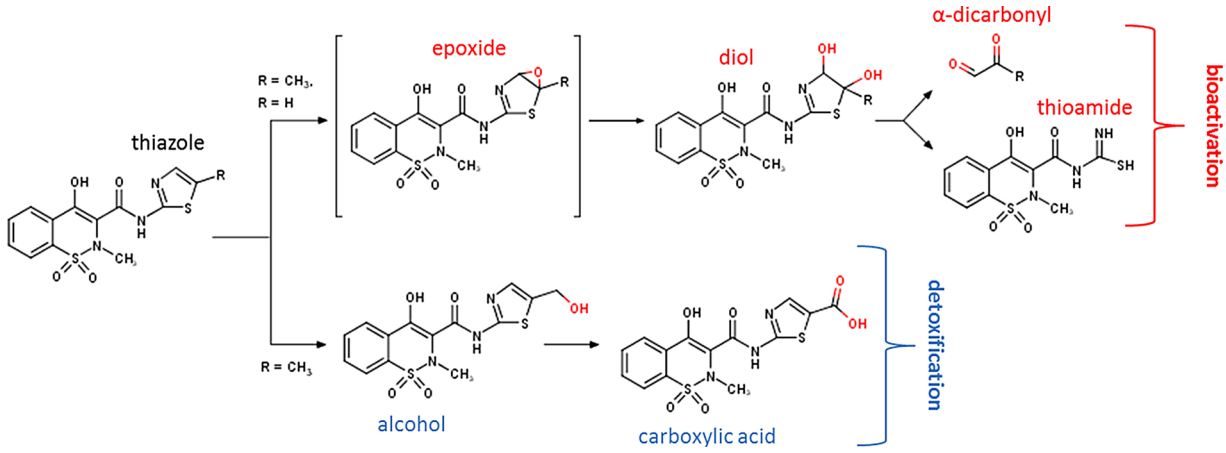

Scheme 1. Metabolic pathways for meloxicam and sudoxicam. Both meloxicam and sudoxicam undergo a bioactivation pathway (red) at the thiazole group initiated by epoxidation of the C4-C5 double bond, followed by hydrolysis and ring cleavage forming the protoxin thioamide and an alpha-dicarbonyl. Meloxicam undergoes a unique detoxification pathway (blue) in which its C5 methyl group is hydroxylated. The metabolite can be directly eliminated or further oxidized and eliminated as a carboxylic acid. (For interpretation of the references to colour in this figure legend, the reader is referred to the web version of this article).

isozymes (Scheme 1). Treatment of mice with general P450 inhibitors methoxsalen and piperonyl butoxide, blocked thiabendazole toxicity (Mizutani et al., 1990, 1992) In a follow-up study, chemical traps isolated thioamide and alpha-dicarbonyl metabolites from thiazole-containing compounds due to microsomal epoxidation at the 4, 5 carbon-carbon double bond. Epoxide hydrolysis yields a diol, and subsequent cleavage of the ring yields thioamide and alpha-dicarbonyl metabolites (Dalvie et al., 2002; Mizutani et al., 1994a). The thioamide is a protoxin which induces toxicity directly or indirectly through oxidized metabolites (Neal and Halpert, 1982; Stigliani and Bernardes-Genisson, 2019). The likelihood for thiazole bioactivation and subsequent toxicity ultimately depends on the structure of the molecule, yet our understanding of those relationships remains woefully inadequate.

A clinically relevant example of a thiazole “soft spot” impacting toxicity is the case of Mobic (meloxicam) and sudoxicam (Jean and Fotsch, 2012). These non-steroidal anti-inflammatory drugs (NSAIDs) have nearly identical molecular structures; sudoxicam possesses a hydrogen at the C5 position whereas a methyl is present for meloxicam. This difference in a thiazole substituent leads to significantly different outcomes for patients. The anti-inflammatory potential of sudoxicam was discovered in the 1970s (Wiseman and Chiaini, 1972), yet follow-up clinical trials led to its withdrawal due to severe hepatotoxicity. Nearly three decades later, the derivative meloxicam was developed and demonstrated a much lower toxicity profile, leading to its approval to treat osteoarthritis in 2000 (Yocum et al., 2000) and later for rheumatoid arthritis in 2004 (Ahmed et al., 2005). This achievement marked the first NSAID that preferentially targets COX-2 and causes fewer gastrointestinal adverse effects compared to other NSAIDs (Ahmed et al., 2005). The drug has only been linked to rare, mild cases of liver damage (“LiverTox”, 2018; Staerkel and Horsmans, 1999; Rostom et al., 2005) in 20 years on the market. Interestingly, both meloxicam and sudoxicam undergo metabolic bioactivation of the thiazole, yet the meloxicam C5 methyl also undergoes hydroxylation in a unique competing detoxification pathway (Schmid et al., 1995; Obach et al., 2008) not possible for sudoxicam. We hypothesized that thiazole bioactivation efficiency is similar between sudoxicam and meloxicam due to the methyl group being a weak electron donator, and thus, the relevance of bioactivation and likely toxicity depends on the competing detoxification pathway. A test of this hypothesis requires knowledge of the kinetics determining bioactivation and, in the case of meloxicam, competing detoxication of the drugs; however, only the efficiency of meloxicam hydroxylation is known (Chesne et al., 1998).

Herein, we combined computational and experimental approaches to interrogate how the difference of a methyl group impacted the intrinsic and relative thiazole bioactivation of sudoxicam and meloxicam. For a rapid analysis, we used our deep-learning epoxidation model to predict their bioactivation and observed no significant difference. As validation, we assessed model capacity to differentiate substituent effects on bioactivation of a diverse array of 68 sudoxicam derivatives with substituents at the C4 or C5 thiazole positions. We then analyzed the effect of electron density from donating and withdrawing groups on predicted bioactivation of the molecules. Inference of electron density relied on the general properties of the substituents, bond order of the site of epoxidation and pKa of the thiazole. The accompanying *in vitro* experimental studies required a far deeper and labor-intensive analysis, and so these efforts focused on revealing only the impact of the thiazole methyl group on bioactivation kinetics between sudoxicam and meloxicam. This analysis required novel applications of sensitive labeling techniques for quantitatively measuring metabolites generated along the pathways (Scheme 1). We leveraged those tools to determine steady-state kinetic mechanisms and constants describing bioactivation and detoxification of the drugs using human liver microsomes. Given these findings, we assessed the performance of our epoxide model in predicting the impact of the methyl group on thiazole bioactivation. Lastly, we analyzed the intrinsic bioactivation kinetics for both drugs and its relative significance for meloxicam by taking into account the competing detoxification pathway as a test of our hypothesis.

2. Experimental Section

2.1. Materials

Chemical solvents methanol, acetonitrile, and DMSO were purchased from Thermo Fisher Scientific (Waltham, MA). Meloxicam, glyoxal and methylglyoxal (metabolites), 7-hydroxycoumarin (internal standard) and 1-aminobenzotriazole (CYP inhibitor) were purchased from Millipore-Sigma (Burlington, MA). Sudoxicam, 5′-hydroxymethyl 5′-desmethyl meloxicam (metabolite), fluoxetine hydrochloride (internal standard), 1,2-diamino-4,5-methylenedioxybenzene dihydrochloride (labeling agent), and dansyl glutathione (trapping agent) were obtained from Toronto Research Chemicals (Toronto, ON, Canada). Epoxide hydrolase inhibitor elaidamide was purchased from Santa Cruz Biotechnology (Dallas, TX). Human liver microsomes pooled from 150 donors (HLM150) were purchased from Corning Gentest (Woburn, MA).

2.2. Epoxidation model

The proposed thiazole bioactivation pathway involves an initial epoxidation of the C4-C5 double bond, and thus, we employed our deep-learning epoxidation model for high-throughput prediction of the impact of thiazole substituents on bioactivation. We constructed and trained a neural network model of epoxidation using data from a previous publication (Abadi et al., 2015) with an improved model architecture. The model's inputs consisted of topological descriptions of atoms, bonds and molecules extracted from the original dataset of 524 molecules. Full details of the descriptors and reaction data used can be found in prior work (Hughes et al., 2015). Briefly, atom descriptors included atom type, the hybridization of the atom, formal charge, the number of implicit hydrogens, and the number and percentage of atoms of each type at distances from 0 to 5 bonds away from the described atom. Bond descriptors included bond order and aromaticity. Molecular descriptors included log octanol-water partition coefficient, molecular weight, total polar surface area, number of hydrogen bond donors and acceptors, number of atoms, and number of bonds of each type. We excluded the quantum chemical descriptors and coordinate-dependent descriptors used in the original study. Given descriptor vectors of each bond, consisting of atom descriptor vectors A1 and A2, bond descriptor vector B, and molecular descriptor vector M, the model computed epoxidation scores as

$$\text{score} = h(f(A1, A2) + f(A2, A1), g(B, M)),$$

where f and g are single fully connected layers with 8 outputs and tanh activation and h is another fully connected layer with 1 output and sigmoid activation. Commas represent vector concatenation. The output score ranged between zero and one and represents the probability that a given bond undergoes an epoxidation reaction. These bond-level epoxidation scores are invariant to the ordering of atoms in the molecule. The model was constructed using the Tensorflow (Abadi et al., 2015) and tflon (Matlock et al., 2019) machine learning toolkits, and was trained by minimizing the cross entropy loss using the SciPy L-BFGS-G optimizer (Zhu et al., 1997; Jones et al., 2020) for 300 iterations. The model was evaluated by leave-one-cluster-out cross-validation as described in the original publication (Hughes et al., 2015). The model achieved an 87.4% top-two accuracy, which is an improvement over the original publication's reported 83% top-two accuracy.

Sudoxicam served as a scaffold for 68 derivatives constructed with 34 different substituents at the C4 or C5 position on the thiazole. The predictions for molecules were compared to the general electron-withdrawing or donating properties of substituents. For a more specific analyses, we compared model predictions to the inferred electron density of the C4-C5 double bond or the thiazole ring itself. For the bonds undergoing epoxidation, we predicted the bond orders for the sudoxicam derivatives using a quantum mechanical (QM) model (Supporting Information, S2). For the thiazole, we inferred electron density by predicting the pKa value of its nitrogen using MarvinSketch (ChemAxon). We then assessed the correlation between the epoxidation model prediction scores and inferred electron density based on QM model predicted bond order or pKa by fitting data to a linear regression using GraphPad Prism 7.0 from GraphPad Software, Inc (San Diego, CA).

2.3. Steady-state metabolism of meloxicam and sudoxicam

We assessed metabolism of meloxicam and sudoxicam using HLM150 as a model for the average adult liver. Due to poor solubility, substrates required the cosolvent DMSO for reactions and thus, control experiments were used to identify an optimal DMSO cosolvent concentration (Supporting Information, S3). Next, we established steady-state conditions for reactions by confirming linear formation of metabolites over time and enzyme concentration (Supporting Information, S4).

Based on these initial studies, the optimal conditions for steady-state studies were determined to be 0.5 mg/mL HLM150 for sudoxicam and meloxicam. Reactions were conducted with varying substrate concentrations and initiated with NADPH regenerating system (0.4 U/mL glucose-6-phosphate dehydrogenase, 3.3 mM glucose 6-phosphate, 3.3 mM $MgCl_2$, 1.3 mM NADP+) in 50 mM potassium phosphate buffer (pH 7.4) at 37 °C with shaking at 350 rpm. Reactions were quenched at 40 min with 2-fold volume of ice cold methanol containing internal standards (10 μM 7-hydroxycoumarin for HPLC-fluorescence and 100 μM fluoxetine for LC–MS analysis) and incubated on ice for 5 min to optimize precipitation of proteins. After 2500 rpm centrifugation (900 xg) to pellet proteins at 4 °C for 15 min using a Thermo Scientific Sorvall ST 40R Centrifuge, the supernatants were transferred to a 96 well half-volume microplate and evaporated to dryness using an Organomation Microvap Nitrogen Evaporator System (Organomation Associates, Inc, Berlin MA). Dried wells were then treated with DMB (for alpha-dicarbonyl analysis samples only) and suspended in mobile phase (20% acetonitrile, 80% water + 0.1% formic acid) for HPLC analysis with fluorescence detection (vide infra). Each set of steady-state reactions was performed in triplicate and replicated four to seven times.

The initial rates from these steady-state reactions were plotted against substrate concentration and then fit to the Michaelis-Menten equation (hyperbolic curve), a biphasic model of two Michaelis-Menten functions, or a biphasic model consisting of a Michaelis-Menten function and a linear function using GraphPad Prism 6.0 (GraphPad Software Inc., San Diego, CA). The best-fit metabolic model and corresponding kinetic constants were determined using Akaike's Information Criterion for small sample sizes (AICc).

2.4. Reaction with inhibitors to identify catalyzing enzymes

Steady-state reactions with inhibitors were used to qualitatively identify enzyme classes that catalyze the thiazole bioactivation pathway. Inhibitors used were 1 μM elaidamide to inhibit microsomal epoxide hydrolase (Morisseau et al., 2001) and 1 mM 1-aminobenzotriazole (ABT) to target general cytochromes P450 (de Montellano, 2018). Individual inhibitor solutions were prepared in potassium phosphate buffer at pH 7.4 with < 0.1% methanol (final) as a co-solvent. Reactions with elaidamide contained 40 and 400 μM substrate, while those with ABT inhibitor were preincubated with HLM for 30 min before initiation with addition of NADPH regenerating system and 400 μM substrate. Reactions without inhibitors but still containing an equivalent concentration of methanol cosolvent served as a baseline for measuring inhibitor effect. Alpha dicarbonyl metabolites were measured using DMB labeling. Statistical differences in normalized rates due to inhibitor presence were determined using the Student's *t*-test (p-value = 0.05).

2.5. Nucleophilic trapping for epoxide intermediates

Thiazole bioactivation into epoxide intermediates is inferred from observed metabolites, but attempts to reveal these epoxides directly or indirectly through glutathione trapping techniques have been unsuccessful (Mizutani et al., 1994a; Obach et al., 2008). We expanded on those efforts for sudoxicam and meloxicam by incubating reactions with four other trapping agents, i.e. dansyl glutathione, dansyl mercaptan, N-acetyl cysteine, and N-acetyl lysine. Reactions with 200 μM substrate and 1 mM epoxide trapping agent in 0.5 mg/mL HLM were initiated with an NADPH regenerating system for a 40 min incubation using same work up method as described previously. Reaction aliquots were quenched by adding 2-fold volume of ice-cold methanol containing dansyl amide as an internal standard. The supernatants were separated from the protein pellet, dried, and resuspended in mobile phase (20% acetonitrile, 80% water + 0.1% formic acid) for HPLC analysis

(Supporting Information, S5). For further validation of putative epoxides, sudoxicam and meloxicam HLM reactions were conducted with epoxide hydrolase inhibitor elaidamide (1 μM) (Morisseau et al., 2001) to facilitate epoxide accumulation and suppression of downstream alpha-dicarbonyl metabolites.

2.6. 1,2-Diamino-4,5-methylenedioxybenzene labeling of alpha-dicarbonyl compounds

1,2-Diamino-4,5-methylenedioxybenzene (DMB) was used as a fluorescent label for sensitive and quantitative detection of alpha-dicarbonyl metabolites after modifying a method developed by others (Ogasawara et al., 2016). Previously described dried reaction samples were resuspended in acetonitrile and combined with an equal volume of water containing 1.0 M β-mercaptoethanol, 28 mM sodium hydrosulfite, and 7.0 mM DMB for a total reaction mixture of 40 μL. Mixtures were incubated at 60 °C for 40 min for labeling and then quenched by diluting 20-fold in mobile phase for HPLC analysis (20% acetonitrile, 80% water + 0.1% formic acid).

2.7. Analysis of fluorescent labeled alpha-dicarbonyl metabolites by HPLC

The resolution and quantitation of DMB labeled alpha-dicarbonyl metabolites glyoxal and methylglyoxal was achieved through high performance liquid chromatography (HPLC). Metabolites were resolved using a 4.6 x 150 mm XSelect 3.5 μM HSS T3 column heated to 45 °C and a Waters HPLC Breeze system equipped with a 2475 Multi λ Fluorescence Detector (Milford, MA). The labeled alpha-dicarbonyl metabolites were resolved using two separate gradient methods with 0.1% formic acid/H_2O (solvent A) and 0.1% formic acid/acetonitrile (solvent B). Glyoxal was resolved over 13 min using a gradient method at 1.0 mL/min starting with 68% A for the first 4 min, followed by linear decrease to 10% A over 1 min. This ratio was maintained for 1 min, and then linearly returned to 68% A over 1 min and held for the remainder of the run. Methylglyoxal was resolved over 13 min using a gradient method at 1.0 mL/min starting with 75% A which was decreased linearly to 70% A for the first 5 min, followed by linear decrease to 20% A over 1 min. The ratio was maintained for 1 min, and then linearly returned to 75% A over 1 min and held for the remainder of the run. All samples were monitored by fluorescence (excitation: 325 nm; emission: 393 nm), and peak areas normalized to internal standard (7-hydroxycoumarin). Reaction responses were corrected for background signals based on analysis of reactions lacking thiazole containing substrates. Glyoxal and methylglyoxal standard curves were used to quantitate the corrected peak areas. High background signals caused high variability for final quantitated rates, so kinetic experiments had to be repeated many times (9–24 replicates per substrate concentration) to maximize confidence in average rate calculations and kinetic curves. Reaction rates were reported as total product formed per reaction time per amount of protein (pmoles/min/mg protein).

2.8. Analysis of 5-hydroxymethyl-meloxicam metabolites by UHPLC-MS

The resolution and quantitation of 5-hydroxymethyl-meloxicam metabolite from meloxicam reactions was achieved using LC–MS analysis based on mass to charge ratio (368 m/z) and co-elution with authentic standards. Metabolites were resolved using a Cortecs C-18 2.7 μm column (4.6 x 50 mm) and a Waters Acquity Arc UHPLC system followed by detection with a Waters Acquity QDa single quadrupole MS system (Milford, MA). Total flow rate was 0.5 mL/min and run time was 20 min. QDa cone voltage was 20 V to detect m/z from 150 to 650 in positive ion mode. The mobile phase comprised two solvents: 0.1% formic acid/H_2O (solvent A) and 0.1% formic acid/acetonitrile (solvent B). The gradient method began at 90% A for 1 min and decreased to 10% A over 11 min. Ratio was maintained at 10% for 4 min, followed by increase back to 90% A over 1 min, which was maintained for remainder of run. Analyte peak areas were normalized to the internal standard (fluoxetine) and quantitated relative to an authentic standard.

3. Results

3.1. General electron donating/withdrawing properties of substituents weakly corresponded to modeled epoxidations

As the first step in bioactivation, we modeled epoxidation of the C4-C5 double bond for 68 variants of sudoxicam differing in substituents at the C4 or C5 position on the thiazole. We initially used the publicly available Xenosite Epoxidation 1.0 (Hughes et al., 2015) model to predict likelihood for epoxidation and observed random oscillation between two different outputs for each molecule. We traced the issue to random selection of two paths for atom numbering that impacted the reported outcome. As described in Methods, we modified the model such that outputs were invariant to atom numbering and made other changes based on current experience with optimizing model design by our group. A leave-one-cluster-out cross-validation revealed that the revised epoxidation model achieved an 87.4% top-two accuracy, which is an improvement over the original model (83%) (Hughes et al., 2015). We then used the revised epoxidation model to predict metabolism of the sudoxicam derivatives. The model predicted similar high metabolic outcomes ($P > 0.99$) for sudoxicam and meloxicam targeted in experimental studies (Fig. 1).

For the class of 68 test molecules, we expected higher electron density to increase the likelihood for epoxidation, and thus, we compared metabolism predictions against the electron-donating and -withdrawing strength of the substituent groups, i.e. strong, moderate, and weak electron-donating and -withdrawing. Nevertheless, this assessment revealed a weak possible positive correlation between epoxidation and theoretical electron density for the C5 substituents (Fig. 2, Panel A) and data points tended to cluster. A correlation was less apparent for C4 substituents (Supporting Information, S7, Panel A).

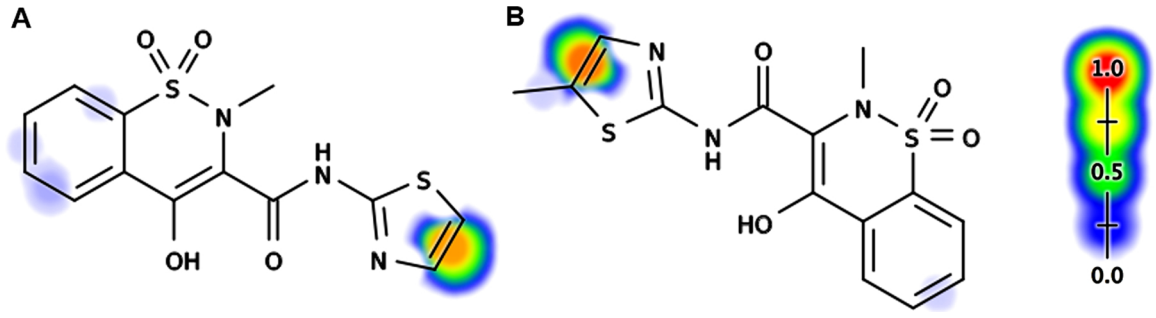

Fig. 1. Thiazole test compounds with epoxidation model predictions. Epoxidation predictions made using the Xenosite epoxidation model 2.0 for sudoxicam (*Panel A*) and meloxicam (*Panel B*). Individual bonds are scored from 0 to 1, with higher scores indicating higher likelihood of epoxidation.

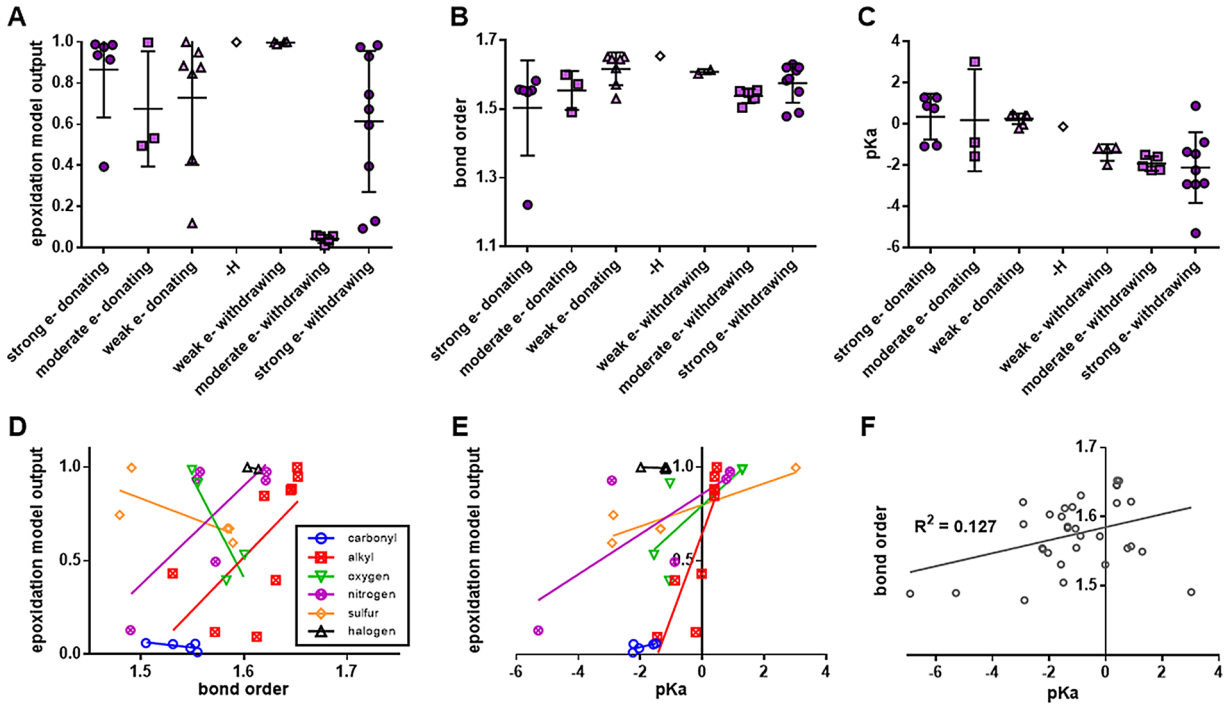

Fig. 2. Epoxidation model outputs versus electron density of sudoxicam C5 substituted derivatives. Sudoxicam derivatives were digitally constructed with 34 different substituents at the C5 position of the thiazole ring. *Panel A*: Epoxidation model outputs (y-axis) were grouped based on electron-donating/withdrawing strength of the C5 thiazole substituent (x-axis). *Panel B:* QM model predicted C4-C5 bond orders (y-axis) were grouped based on electron-donating/withdrawing strength of the C5 thiazole substituent (x-axis). *Panel C*: pKa predictions for the thiazole nitrogen atom (y-axis) were grouped based on electron-donating/withdrawing strength of the C5 thiazole substituent (x-axis). *Panel D*: Epoxidation model outputs (y-axis) were plotted as a function of QM model bond order predictions (x-axis) with points grouped based on identity of the alpha position atom. *Panel E*: Epoxidation model outputs (y-axis) were plotted as a function of pKa predictions for the thiazole nitrogen atom (x-axis) with points grouped based on identity of the alpha position atom. *Panel F*: QM model predictions (y-axis) and pKa values (x-axis) were plotted for comparison.

3.2. QM modeling of the bond undergoing epoxidation did not reflect a relationship with modeled epoxidations

In a more detailed analysis, we explored relationships between inferred electron density for test compounds and epoxidation predictions. First, we used a WAVE-based QM model to predict the bond order at the C4-C5 double bond targeted for epoxidation except molecules containing bromine and iodine due to their absence in the basis set (see Methods). The WAVE model is more complex than the epoxidation model, capable of modeling long range and non-linear interactions more effectively. Based on chemical reasoning, we expected higher bond order predictions with electron donating substituents, but instead we observed that the predicted bond order was the highest for the unsubstituted scaffold compound, with electron density decreasing with increasing strength of electron-donating and -withdrawing groups at the C5 position (Fig. 2, Panel B) and the C4 position to a lesser extent (Supporting Information, S7, Panel B); these findings suggest a more complex relationship between the substituents and bond order than our initial intuition. In this series, bond electron density and epoxidation model predictions did not reveal a strong correlation with one another (Table 1). The breakdown of substituents into groups based on the atom attached to the ring revealed trends in the data, but they were not consistent across the groups for both C5 (Table 1, Fig. 2, Panel D) and C4 (Supporting Information, S6, S7, Panel D). The trendline slopes were positive, negative or essentially zero, so that bond electron density of the QM model did not correlate with epoxidation model predictions. This finding was surprising, because bond electron density correlated with epoxidation likelihood across the whole epoxidation dataset (Hughes et al., 2015).

Table 1
Epoxidation Model Output Linear Correlations with Electron Density for Sudoxicam C5 Substituted Derivatives.

		bond order			pKa		
	n	slope	R square	F-test (p value)	slope	R square	F-test (p value)
total	34	2.965	0.1896	0.0100	0.088	0.191	0.007
carbonyl	5	−0.6147	0.3955	0.2557	0.036	0.3983	0.2535
alkyl	9	5.696	0.4261	0.0566	0.4476	0.7119	0.0042
nitrogen	6	5.286	0.5491	0.0919	0.1071	0.6014	0.0699
oxygen	5	−10.58	0.7704	0.1223	0.1514	0.5697	0.1403
sulfur	5	−2.097	0.5666	0.1420	0.05723	0.8039	0.0393
halogens	4[a]	NA[a]	NA	NA	−0.005327	0.2118	0.5373

[a] Bond order predictions could not be yielded for those molecules that contained either bromine or iodine, so only two halogen bond order predictions were possible.

3.3. Electron density inferred from thiazole pKa correlated with epoxidation predictions

We used pKa predictions as a second comparison point. We predicted the thiazole pKa of the sudoxicam derivatives using MarvinSketch (ChemAxon) and used those values as descriptors of electron density for the overall thiazole ring. The ChemAxon pKa model is based on a substructure electronegativity model and does not capture complex long-range effects. For this reason, it is more likely to match the representation of the epoxidation model than the QM model. Consistent with chemical intuition, electron-withdrawing C5

substituents resulted in lower pKa values overall, while values were slightly higher for electron-donating C5 substituents (Fig. 2, Panel C). The trend was not observed for C4 substituents, suggesting a less important impact on pKa (Supporting Information, S7, Panel C). Unlike the bond order predictions, increasing pKa values positively correlated with epoxidation scores for nearly all C5 (Table 1, Fig. 2, Panel E) and C4 (Supporting Information, S6, S7, Panel E) substituent groups except the halogens. The pKa values were then more reflective of epoxidation predictions than bond order predictions. Despite those correlations, scaling between substituent types was not consistent given variations in slopes and some substituent effects were not predictive at all (halogens).

Lastly, we assessed the relationship between C4-C5 bond order predictions and thiazole pKa and found no correlation for C5 (Fig. 2, Panel F) or C4 (Supporting Information, S7, Panel F) substituents. This finding is consistent with the lack of correlation between bond order predictions and epoxidation model scores. The QM model may be better at capturing long-range interactions in molecules (Matlock et al., 2019) yielding a more complex chemical readout of reactivity than the usual chemical reasoning embodied by the simpler epoxidation or pKa models.

3.4. Multiple enzyme types catalyze thiazole bioactivation depending on drug structure

The thiazole bioactivation pathway begins with formation of an epoxide that undergoes cleavage to a dihydrodiol and then breakdown into a thioamide and alpha-dicarbonyl (Scheme 1). Like others (Mizutani et al., 1994a; Obach et al., 2008), we were not able to directly observe epoxides or downstream dihydrodiol metabolites of sudoxicam and meloxicam generated from HLM reactions using MS analyses. We then tried trapping epoxides using nucleophilic traps, i.e. dansyl glutathione, dansyl mercaptan, N-acetyl cysteine and N-acetyl lysine, to form stable, observable adducts, yet the analysis of those reactions by MS and fluorescence yielded negative results. The lack of detectable epoxides may reflect rapid decay under reaction conditions, and thus, we repeated HLM reactions with the epoxide hydrolase inhibitor elaidamide. Again, neither of the epoxide metabolites were observed directly or indirectly using the trapping reagents. These observations could reflect limitations of our methods and thus, we assessed the impact of elaidamide on downstream measurable metabolites of the bioactivation pathways, i.e. the alpha-dicarbonyls as measured by DMB labeling (Fig. 3, Panel A). Interestingly, elaidamide significantly inhibited (90%) glyoxal formation from sudoxicam, yet the metabolism of meloxicam into methylglyoxal was not affected by the inhibitor, suggesting the epoxide hydrolase plays a role in breakdown of the sudoxicam epoxide but not the one derived from meloxicam (Fig. 3, Panel B). Preincubation with ABT inhibitor resulted in significant inhibition of alpha-dicarbonyl formation from both sudoxicam (75% inhibition) (Fig. 3, Panel C) and meloxicam (85% inhibition) (Fig. 3, Panel D), suggesting cytochromes P450 involvement in the bioactivation pathways of both drugs.

3.5. Fluorescently labeled glyoxal and methylglyoxal yielded sensitive, robust metabolic endpoints for bioactivation

Despite challenges observing the epoxide and dihydrodiol metabolites, we were able to measure the alpha-dicarbonyl cometabolite of the thioamide protoxin (Scheme 1). We adapted a method reported by others (Ogasawara et al., 2016) to react DMB with glyoxal from sudoxicam and methylglyoxal from meloxicam, to generate a fluorophore. Background peaks from HLM reactions coeluted with labeled glyoxal and methylglyoxal (data not shown), so that final analyte values required correction with the appropriate blank reactions. Based on five standard curves, the limits of detection were 90 nM for methylglyoxal and 80 nM for glyoxal, as calculated by three times the standard deviation of the normalized peak areas of the lowest concentration divided by the average slopes of the standard curves. Importantly, these metabolites were stable under reaction conditions. At low (50 μM) and high (500 μM) concentrations, glyoxal showed no significant depletion, and methylglyoxal only significant depletion after 60 min based on student's *t*-test ($p < 0.05$) (Supporting Information, S8).

3.6. Methyl group significantly impacted metabolic kinetics for meloxicam and sudoxicam

Steady state reactions were conducted to determine the mechanism and constants describing the metabolic conversion of sudoxicam to glyoxal and meloxicam to either methylglyoxal or 5-hydroxymethyl-meloxicam. As an initial step, we assessed the linearity in observed rates at low (40 μM) and high (400 μM) substrate concentrations as a function of time (Supporting Information, S9) and protein concentration (Supporting Information, S10). Based on those data, the optimal steady-state conditions for all targeted metabolites were 0.5 mg/mL HLM and a 40 min reaction time, and thus, those conditions were used for kinetic experiments for the drugs. The resulting kinetic profiles were then fit to single or biphasic kinetics models to determine the most probable mechanisms and constants for reactions using corrected Akaike information criterion.

The difference in a methyl group between sudoxicam and meloxicam led to different mechanisms describing bioactivation and detoxification of the drugs (Table 2). The metabolic pathway for sudoxicam leading to glyoxal was best fit to a biphasic model for two enzyme activities. A high affinity phase fit to the Michaelis-Menten mechanism (V_{max1}/K_{m1} 2.2) and was followed by a second non-saturable linear phase with a 100-fold lower efficiency for the reaction (V_{max2}/K_{m2} 0.021) (Fig. 4, Panel A). Metabolism of meloxicam into methylglyoxal demonstrated a single metabolic phase that fit best to the Michaelis-Menten mechanism (Fig. 4, Panel B). The efficiency of this bioactivation pathway (V_{max}/K_m 0.32) was 7-fold lower than that for sudoxicam. These differences reflect a lower V_{max} and much higher K_m for the reaction, so that the methyl group suppressed the bioactivation pathway. The competing meloxicam detoxification pathway yielding 5-hydoxymethyl-meloxicam followed a biphasic model, in which one phase fit Michaelis-Menten kinetics and the other did not saturate within our experimental range (Fig. 4, Panel C). The high affinity phase led to the most efficient metabolic reaction in this study (V_{max1}/K_{m1} 1.9) and at higher substrate concentrations, a second 130-fold less efficient activity contributed to turnover (slope 0.014). Given similar V_{max} values for the activities, the difference arose solely from substrate binding as reflected in the respective K_m values. When compared to the meloxicam bioactivation pathway, the high affinity detoxification reaction was 6-fold more efficient. The pathways would compete, leading to meloxicam partitioning down the two possibilities based on their efficiencies. The actual metabolic flux of meloxicam bioactivation is then the ratio of bioactivation efficiency over the sum of both reaction efficiencies, or 0.14. Based on that knowledge, sudoxicam is ~15-fold (2.2/0.14) more efficiently bioactivated than meloxicam.

4. Discussion

4.1. Epoxidation predictions reflected electron density but did so unevenly among substituents

The toxic potential of thiazoles begins with the initial epoxidation step, and thus, we predicted the relative importance of that reaction for sudoxicam and meloxicam using our epoxidation model (version 1.0) (Dang et al., 2016). The reaction occurs at a double bond, and our epoxidation model is designed to predict the precise bond at which an epoxide is formed. In this study, the application of our original, published model revealed its tendency to generate randomly one of two possible numerical outcomes due to random orientation of the thiazole.

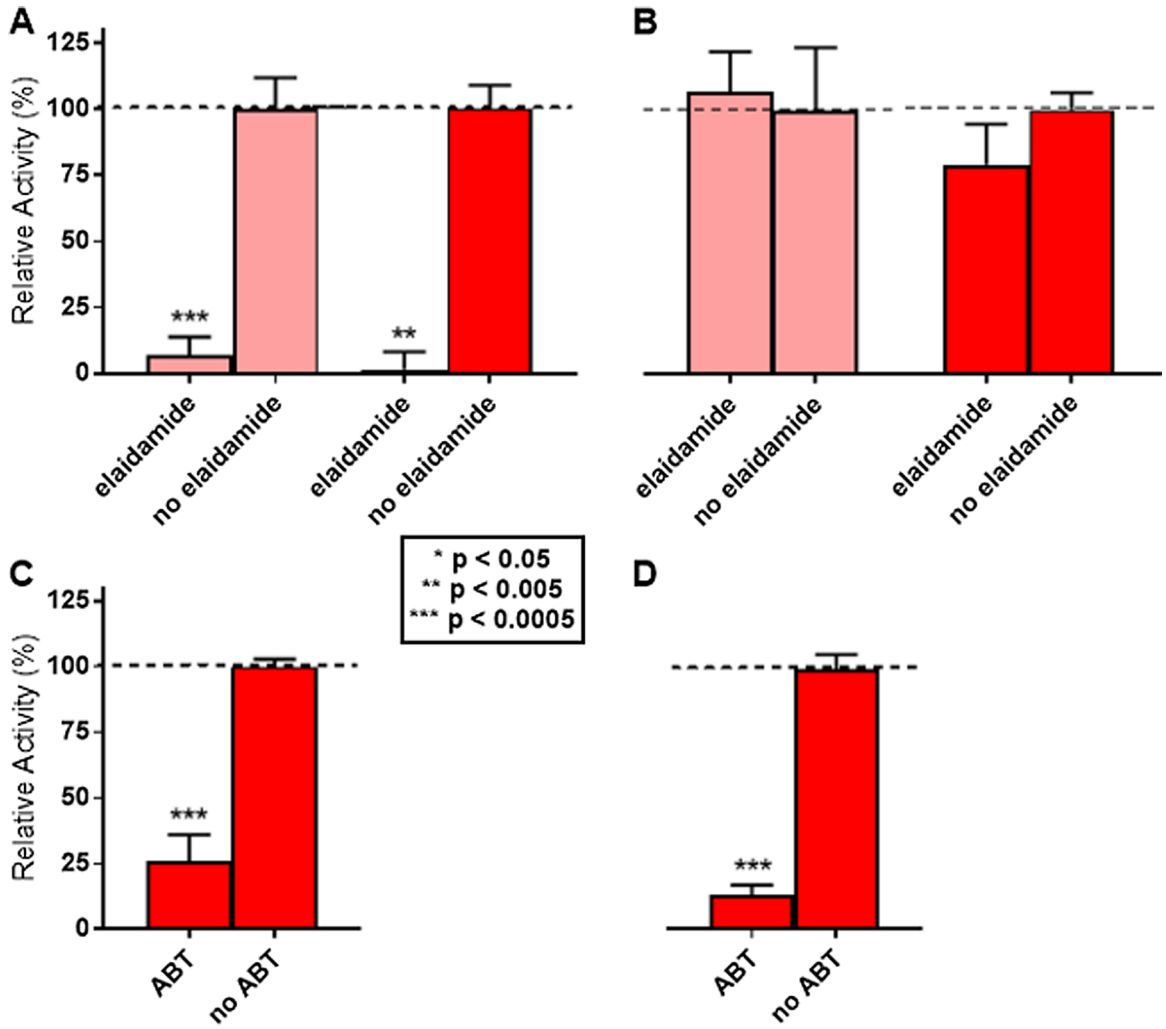

Fig. 3. . Chemical inhibition of bioactivation pathways. As described in Experimental Procedures, alpha-dicarbonyl metabolite formation rates were measured for substrate reactions with human liver microsomes. Sudoxicam (*Panel A*) and meloxicam (*Panel B*) reactions at 40 μM (pink) and 400 μM (red) concentrations were conducted with 1 μM elaidamide for microsomal epoxide hydrolase inhibition. Coincubation with 1 mM 1-aminobenzotriazole was conducted with 400 μM sudoxicam (*Panel C*) and meloxicam (*Panel D*) for general cytochrome P450 inhibition. Each reaction was conducted in six to nine replicates. Alpha-dicarbonyl formation rates are reported as percentages normalized to rates in uninhibited reactions. Average non-inhibited rates (in pmol/min/mg enzyme) were 12 for 40 μM sudoxicam, 21 for 400 μM sudoxicam, 5.0 for 40 μM meloxicam, and 7.6 for 400 μM meloxicam. Significant differences between inhibited reaction rates and the controls were determined based on $p < 0.05$ calculated using Student's *t*-test. Error bars denote standard error. (For interpretation of the references to colour in this figure legend, the reader is referred to the web version of this article).

This design flaw impacted predictions of metabolism at double bonds but not atoms, so that it is not a problem for our other metabolism models. We resolved the issue and made other improvements to the model (Methods). The new epoxidation model (version 2.0) demonstrated better performance than the original model and will be made freely accessible through Xenosite (https://swami.wustl.edu/xenosite). Using the improved model, we found that the difference in a methyl group between meloxicam and sudoxicam did not impact the likelihood for epoxidation, suggesting the electron donating ability of the methyl group was not important in this metabolic step. Nevertheless, both

Table 2
Michaelis-Menten Kinetic Constants for Sudoxicam and Meloxicam Metabolites from Human Liver Microsome Reactions.

		Steady-state kinetic constants for individual metabolites[a]					
Substrate	Metabolite	$V_{max}1$[b]	K_m1 (μM)	V_{max}/K_m1	$V_{max}2$[b]	K_m2 (μM)	V_{max}/K_m2
sudoxicam	glyoxal	13 ± 0.75	5.9 ± 1.2	**2.2**	NA	NA	**0.021**[c]
meloxicam	methylglyoxal	8.4 ± 0.39	26 ± 4.9	**0.32**	NA	NA	**NA**
	5-hydroxymethyl-meloxicam	29 ± 2.0	15 ± 2.9	**1.9**	NA	NA	**0.014**[c]
		34 ± 24[d]	14 ± 9.5[d]	**2.4**	140 ± 84[d]	380 ± 55[d]	**0.37**

[a] Best fit models shown in Fig. 4 were determined using corrected Akaike information criterion. Values shown with standard error from mean.
[b] Units are pmol/min/mg protein.
[c] Efficiency estimated based on slope of linear function.
[d] Data reported by others (Chesne et al., 1998).

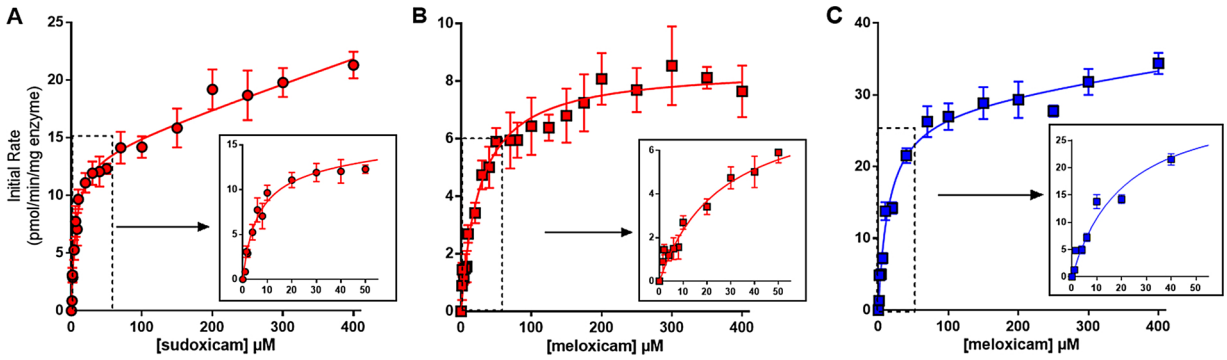

Fig. 4. Steady state kinetic profiles for metabolites of sudoxicam and meloxicam. Alpha-dicarbonyl metabolites from the thiazole bioactivation pathway were observed for sudoxicam and meloxicam reactions by human liver microsomes. Glyoxal (red circles) from sudoxicam (*Panel A*) and methylglyoxal (red squares) from meloxicam (*Panel B*) were detected using DMB labeling. The 5-hydroxymethyl-meloxicam metabolite (blue squares) from the meloxicam detoxification pathway (*Panel C*) was measured by mass detection (*m/z* 368). Metabolites were quantitated using standard curves to calculate initial rates (pmol/min/mg protein) as a function of substrate concentration (μM). Data for all reactions were fit best to a biphasic Michaelis-Menten equation or a single Michaelis-Menten equation using Akaike information criterion for small sample sizes (AICc), and the corresponding constants are reported in Table 2. Experimental reactions for each substrate concentration were replicated between nine and twenty-four times. Analysis was conducted as described in Materials and Methods. (For interpretation of the references to colour in this figure legend, the reader is referred to the web version of this article).

predictions were very high for the reaction, so that it was unclear if the model was able to scale the effects of substituents on thiazole epoxidation or not.

Consequently, we interrogated model predictions for 68 different sudoxicam derivatives possessing various substituents and assessed the relationships between those structural differences and predicted epoxidations. These reactions would most likely be carried out by cytochrome P450 isozymes (Mizutani et al., 1990, 1992), whose primary oxidant is an electrophilic perferryl species (FeO^{3+}) (Higson, 2012). Epoxidation of thiazoles would then positively correlate with higher electron density. There was only a weak relationship between model predictions and substituents when grouped based on relative electron-donating and -withdrawing properties. Moreover, data point clustering suggested subpopulations of substituents shared similar properties. This analysis was clearly not sufficient to study the basis for model predictions; a more granular analysis was necessary.

We more specifically inferred electron density for correlative analyses of model predictions in two ways. First, we relied on bond order based on Quantum Mechanical calculations as a measure of the electron density for the thiazole C4-C5 double bond. The bond order predictions with the WAVE model yielded a surprising relationship with the substituents grouped according to electron-donating/withdrawing abilities. Rather than the expected positive correlation, the bond order increased with weaker electron-donating groups and then decreased with strengthening electron-withdrawing groups to create an inflection point with hydrogen as the substituent. There is a precedent for this behavior whereby pi-bond electrons are “pushed and pulled” between an electron-donating group on one carbon and electron-withdrawing group on the other (Kleinpeter, 2006). We analyzed correlations between epoxidation model predictions versus predicted bond electron density on sudoxicam derivatives, grouping by substituent classes defined by the atom directly connected to the thiazole ring. Individual classes of substituents yielded correlations differing in magnitude and sign, such that there was no clear correlation overall between QM model predictions and epoxidation predictions. This result suggests either that the epoxidation model does not rely on bond electron density in this series, or the model is inferring the bond density differently than the QM model.

In contrast, epoxidation scores correlated with predicted pKa to model substituent effects of epoxidation. Thiazole pKa for sudoxicam derivatives positively correlated with increasing electron density (Higson, 2012). This relationship was consistent with the epoxidation model predictions relative to pKa. When broken down by substituent classes, epoxidation model predictions correlated positively with pKa; however, based on the slopes, there was wide variability in the sensitivity of the model prediction to pKa. These differences may be due to differences in how the model scales the effects of substituents on epoxidation predictions. In the case of halogens, the differences in their properties had no impact on model predictions. This observation may reflect the underrepresentation of halogenated drugs in the AMD training set for the model. Even the 23 thiazole-containing molecules present in the data set lack halogens on the thiazole ring. Knowledge of these deficiencies provides a basis for refinement of the model to improve the accuracy and capacity to generalize predictions. Overall, the epoxide model predictions more closely aligned with pKa predictions. The divergence between WAVE model and epoxidation model predictions may reflect complex interactions of thiazole with substituents that is not well captured by simple models. In the long run, the incorporation of QM-based modeling into the epoxidation model could improve predictions for thiazoles.

4.2. Epoxidation hydrolysis was an essential step in the thiazole bioactivation pathway

The general bioactivation pathway for thiazoles is initiated with epoxidation at the thiazole C4-C5 double bond, followed by hydrolysis to form a diol and finally ring cleavage to form an alpha-dicarbonyl and a thioamide protoxin (Mizutani et al., 1994b) (Scheme 1). For sudoxicam and meloxicam, Obach et al. (2008) reported evidence for all metabolites and intermediates in the pathway except for the proposed initial epoxide. Alkene epoxidation is an established metabolic reaction carried out by cytochromes P450 on multiple drugs, comprising up to 15% of all bioactivation reactions (Hughes et al., 2015; Testa et al., 2012), yet the epoxidized thiazole intermediate has never been observed previously either directly or indirectly through the use of glutathione for trapping (Obach et al., 2008; Mizutani et al., 1994a). We obtained the same results for sudoxicam and meloxicam, and thus, we sought to better our odds for observing epoxide metabolites. We blocked the enzymatic breakdown of the epoxide using the epoxide hydrolase inhibitor elaidamide, yet we still detected no epoxides or even epoxide adducts with various trapping agents. This absence may reflect more effective trapping by microsomal proteins (Bu et al., 2005), limits of instrumental detection, and/or ineffectiveness of the inhibitor to impact that reaction step. In fact, there was a nearly complete decrease in glyoxal formation from sudoxicam in the presence of the inhibitor, yet that was not the case for methylglyoxal from meloxicam. This surprising find implicates epoxide hydrolase activity as critical for the sudoxicam, but not meloxicam, metabolic pathway leading to the

alpha-dicarbonyl metabolite. The reason for this difference in outcomes for the two drugs is currently unclear. One possible explanation is that the presence of the methyl thiazole substituent for meloxicam may alter epoxide hydrolase specificity to favor an alternate pathway for breakdown of the metabolite to form eventually alpha-dicarbonyl. Additionally, the meloxicam pathway may be metabolized by a unique isoform of human epoxide hydrolase. For example, EH3 is a recently identified epoxide hydrolase whose activity is associated with the membranous fraction of cell lysate. Unlike the classic microsomal epoxide hydrolase isoform (mEH), EH3 activity is not affected by elaidamide inhibition (Decker et al., 2012).

4.3. Sudoxicam bioactivation pathway was more efficient compared to meloxicam

Despite previous challenges, we are the first to report the microsomal kinetics for the sudoxicam and meloxicam bioactivation pathways based on alpha-dicarbonyl formation rates (Scheme 1). Like meloxicam hydroxylation (Chesne et al., 1998), these oxidative pathways for both drugs involve cytochrome P450 isozymes according to our inhibitory phenotyping studies using ABT. Steady-state kinetics for sudoxicam metabolism into glyoxal was biphasic reflecting high affinity and unsaturable isozyme activities. The significant difference (100-fold) in the reaction efficiencies indicates that only the high affinity activity would likely be relevant at the typical low drug levels observed under biological conditions (Gschwend et al., 2007). The kinetics for sudoxicam bioactivation could reflect a single P450 isozyme given their capacity to display non-hyperbolic kinetics (Lin et al., 2001; Isin and Guengerich, 2016; Niwa et al., 2008) or alternatively, the action of two separate P450 isozymes. The latter possibility seems more plausible based on meloxicam hydroxylation studies in which biphasic microsomal kinetics were shown to reflect contributions by both CYP2C9 and 3A4 (Chesne et al., 1998). A similar combination of two P450 isozymes could contribute to the sudoxicam bioactivation pathway and mediate its relative significance in patients.

We hypothesized that the presence of a weak electron-donating methyl group at the thiazole C5 position would have a minimal effect on epoxidation so that meloxicam and sudoxicam bioactivation kinetics would be similar, but that was not the case. Unlike sudoxicam, meloxicam kinetics for methylglyoxal fit best to Michaelis-Menten mechanism suggesting that a single enzyme bioactivated the drug. The impact of the C5 methyl group on the efficiency of epoxidation was surprisingly very negative, with a 50% lower V_{max} and a four-fold higher K_m for meloxicam compared to sudoxicam. While sterically small, the methyl substituent was capable of significantly decreasing the specificity and affinity of meloxicam bioactivation by P450 s, making the pathway six-fold less efficient than the high affinity one for sudoxicam. The deactivating effect of substituents at the C5 thiazole position has been reported previously. One study showed that bioactivation of a similar heterocyclic five membered ring, thiophene, was decreased by substituents at the C5 position more so than at the C4 position (Chen et al., 2011). In another study, C5 substitutions blocked thiazole bioactivation for a nonpeptidyl thrombopoietin receptor agonist (Kalgutkar et al., 2007), highlighting that site as a thiazole “soft spot” for reactivity (Jean and Fotsch, 2012).

4.4. Meloxicam detoxification was more efficient than bioactivation

The methyl group for meloxicam provides a site of metabolism for a detoxification pathway unavailable for sudoxicam (Scheme 1). The reaction with human liver microsomes is biphasic with a low efficiency reaction and a 130-fold higher efficiency one presumably by CYP3A4 and 2C9, respectively (Chesne et al., 1998). In our study, we recapitulated the published results for the high affinity reaction generating nearly identical values but were not able to saturate a low affinity activity as reported previously (Table 2). This outcome reflected differences in experimental design. The authors of the original study carried out reactions with DMSO concentrations as high as 1.0% to achieve saturation of the low affinity activity. Such levels of DMSO would significantly inhibit CYP3A4 activity (Chauret et al., 1998; Easterbrook et al., 2001) leading to the false impression of enzyme saturation and thus inaccurate kinetics. We avoided that complication by minimizing DMSO use to 0.1% and holding that level constant for all reactions. Lastly, the efficiency of meloxicam detoxification was 6-fold higher than bioactivation; this stark contrast in metabolism reflects differences in the reactivity and/or accessibility of the sites of metabolism despite their proximity.

4.5. Both bioactivation and detoxification pathways likely contribute to differences in clinical sudoxicam and meloxicam metabolism

We approximated overall differences in relative bioactivation for meloxicam and sudoxicam under clinical conditions by comparing their metabolic flux down the competing bioactivation and detoxification pathways. For comparative purposes, we assumed sudoxicam plasma levels reach similar levels in patients as meloxicam, so that the maximal clinical drug levels would be 3.2 μM (Gschwend et al., 2007). Under those conditions, only the high affinity metabolic activities contribute to drug metabolism. Moreover, drug levels remain below the K_m values for bioactivation and detoxification reactions, and thus, kinetic efficiencies (V_{max}/K_m) are accurate descriptions of the relative metabolic flux through those pathways. Unlike sudoxicam, the relative significance of meloxicam bioactivation must take into account partitioning down bioactivation and detoxification pathways. When compared to sudoxicam, the metabolic flux of meloxicam bioactivation is 15-fold less efficient than that for sudoxicam. Taken together, the C5 thiazole methyl group suppressed epoxidation and introduced a detoxification pathway, resulting in decreased bioactivation potential for meloxicam over sudoxicam; such a significant difference in bioactivation could explain the very low incidences of drug-induced liver injury associated with meloxicam over sudoxicam (Obach et al., 2008). The fact that nearly three decades passed between the initial sudoxicam studies (Wiseman and Chiaini, 1972) and the approval of meloxicam as a safer alternative (Yocum et al., 2000) highlights the complexities involved with finding safer alternatives to drugs with even simple modifications, and thus the need to understand the underlying mechanisms that link structure to toxic outcome.

4.6. Experimental bioactivation kinetics implicated importance of the chemical step in model epoxidations

Although limited to sudoxicam and meloxicam, our novel thiazole bioactivation kinetics provide an opportunity to explore the accuracy and meaning of our model predictions. The introduction of the C5 methyl group had minimal effect on modeled epoxidation outcomes and QM modeled bond orders as observed for the corresponding V_{max} values from steady-state studies. This kinetic constant likely reflects the rate-limiting chemical step, which is a common feature of P450 isozyme reactions (Guengerich, 2002). In fact, the correlations of model predictions with pKa support chemical properties of the thiazole as a determinant in model outcomes. Consequently, epoxidation predictions may better align with chemical reactivity than binding contributions from enzymatic reactions and hence, impact their use and interpretation in metabolism studies.

4.7. Concluding remarks

Overall, our combination of computational and experimental approaches revealed the impact of a methyl group on the intrinsic and relative thiazole bioactivation of sudoxicam and meloxicam as well as the potential for modeling to yield insights on the effects of other thiazole substituents. The analysis of our epoxidation model using the

sudoxicam scaffold revealed its strengths in predicting structure-specific chemical reactivity for bonds while highlighting current deficiencies. Furthermore, we used novel applications of analytical techniques for experimental quantitation of the thiazole bioactivation pathway. We gathered new evidence for epoxide formation in the established thiazole bioactivation pathway and for an inhibitory role of C5 methyl substituents on the pathway. Knowledge of the mechanism of substituent effects on thiazole P450 bioactivation and detoxification pathways can benefit drug design and improve clinical outcomes. Future identification of the specific P450 isozymes involved in metabolism could lead to predictions of mild idiosyncratic toxicity, such as those observed for meloxicam ("LiverTox", 2018; Staerkel and Horsmans, 1999; Rostom et al., 2005), on a personalized basis. Finally, broader knowledge of the effect of functional groups on the metabolic fate of the frequently used thiazole scaffold can be used to improve drug design to decrease the likelihood of bioactivation and subsequent toxicity in patients.

Funding

This work was supported by the National Library of Medicine of the National Institutes of Health [grant numbers R01LM012222, R01LM012482]; the National Institute of General Medical Sciences [grant number T32GM106999]; National Institutes of Health (NIH) NCRR [grant numbers 1S10RR022984-01A1, 1S10OD018091-01]; and the University of Arkansas for Medical Science Vice Chancellor of Research Equipment Grant.

Declaration of Competing Interest

The authors declare that they have no known competing financial interests or personal relationships that could have appeared to influence the work reported in this paper.

Appendix A. Supplementary data

Supplementary material related to this article can be found, in the online version, at doi:https://doi.org/10.1016/j.tox.2020.152478.

References

Abadi, M., Agarwal, A., Barham, P., Brevdo, E., Chen, Z., Citro, C., Corrado, G.S., Davis, A., Dean, J., Devin, M., Ghemawat, S., Goodfellow, I., Harp, A., Irving, G., Isard, M., Jia, Y., Jozefowicz, R., Kaiser, L., Kudlur, M., Levenberg, J., Mane, D., Monga, R., Moore, S., Murray, D., Olah, C., Schuster, M., Shlens, J., Steiner, B., Sutskever, I., Talwar, K., Tucker, P., Vanhoucke, V., Vasudevan, V., Viegas, F., Vinyals, O., Warden, P., Wattenberg, M., Wicke, M., Yu, Y., Zheng, X., 2015. TensorFlow: Large-scale Machine Learning on Heterogeneous Distributed Systems.

Ahmed, M., Khanna, D., Furst, D.E., 2005. Meloxicam in rheumatoid arthritis. Expert Opin. Drug Metab. Toxicol. 1, 739–751.

Ayati, A., Emami, S., Asadipour, A., Sha, A., Foroumadi, A., 2015. European Journal of Medicinal Chemistry Recent applications of 1, 3-thiazole core structure in the identification of new lead compounds and drug discovery. Eur. J. Endocrinol. 97, 699–718. https://doi.org/10.1016/j.ejmech.2015.04.015.

Bu, H., Kang, P., Deese, A.J., Zhao, P., Pool, W.F., 2005. Human in vitro glutathionyl and protein adducts of carbamazepine-10,11-epoxide, a stable and pharmacologically active metabolite of carbamazepine. Drug Metab. Dispos. 33, 1920–1924. https://doi.org/10.1124/dmd.105.006866.plored.

Chauret, N., Gauthier, A., Nicoll-griffith, D.A., 1998. Accelerated communication: effect of common organic solvents on in vitro cytochorme p450-mediated metabolic activities in human liver microsomes. Drug Metab. Dispos. 26, 4–7.

Chen, W., Caceres-Cortes, J., Zhang, H., Zhang, D., Humphreys, W.G., Gan, J., 2011. Bioactivation of substituted thiophenes including alpha-chlorothiophene-containing compounds in human liver microsomes. Chem. Res. Toxicol. 24, 663–669. https://doi.org/10.1021/tx100386z.

Chesne, C., Guyomard, C., Guillouzo, A., Schmid, J., Ludwig, E., Sauter, T., 1998. Metabolism of meloxicam in human liver involves cytochromes P4502C9 and 3A4. Xenobiotica 28, 1–13.

Dalvie, D.K., Kalgutkar, A.S., Khojasteh-bakht, S.C., Obach, R.S., Donnell, J.P.O., 2002. Biotransformation reactions of five-membered aromatic heterocyclic rings. Chem. Res. Toxicol. 15. https://doi.org/10.1021/tx015574b.

Dang, N.L., Hughes, T.B., Krishnamurthy, V., Swamidass, S.J., 2016. A simple model predicts UGT-Mediated metabolism. Bioinformatics. https://doi.org/10.1093/bioinformatics/btw350.

de Montellano, P.R.O., 2018. 1-Aminobenzotriazole: a mechanism-based cytochrome p450 inhibitor and probe of cytochrome p450 biology. Med. Chem. (Los Angeles) 8, 38–65. https://doi.org/10.4172/2161-0444.1000495.

Decker, M., Adamska, M., Cronin, A., Giallonardo, F.D., Burgener, J., Marowsky, A., Falck, J.R., Morisseau, C., Hammock, B.D., Gruzdev, A., Zeldin, D.C., Arand, M., 2012. EH3 (ABHD9): the first member of a new epoxide hydrolase family with high activity for fatty acid epoxides. J. Lipid Res. 53, 2038–2045. https://doi.org/10.1194/jlr.M024448.

Easterbrook, J., Lu, C., Sakai, Y., Li, A.P., 2001. Effects of organic solvents on the activitites of cytochrome p450 isoforms, UDP-dependent glucuronyl transferase, and phenol sulfotransferase in human hepatocytes. Drug Metab. Dispos. 29, 141–144.

GlaxoSmithKline, 2007. Fortaz (ceftazidime for injection) [package insert]. U. S. Food and Drug Administration.

Gschwend, M.H., Erenmemisoglu, A., Martin, W., Tamur, U., Kanzik, I., Hincal, A.A., 2007. Pharmacokinetic and bioequivalence study of meloxicam tablets in helathy male subjects. Arzneimittelforschung 57, 264–268.

Guengerich, F.P., 2002. Rate-limiting steps in cytochrome P450 catalysis. Biol. Chem. 383, 1553–1564. https://doi.org/10.1515/BC.2002.175.

Higson, S., 2012. Biosensors for Medical Applications. Elsevier.

Hughes, T.B., Miller, G.P., Swamidass, S.J., 2015. Modeling epoxidation of drug-like molecules with a deep machine learning network. ACS Cent. Sci. 1, 168–180. https://doi.org/10.1021/acscentsci.5b00131.

Isin, E.M., Guengerich, F.P., 2016. Substrate binding to cytochromes P450. Anal. Bioanal. Chem. 392, 1019–1030. https://doi.org/10.1007/s00216-008-2244-0.Substrate.

Jean, D.J.S., Fotsch, C., 2012. Mitigating heterocycle metabolism in drug discovery. J. Med. Chem. 55, 6002–6020. https://doi.org/10.1021/jm300343m.

Jones, E., Oliphant, T., Peterson, P., n.d. SciPy: Open source scientific tools for Python.

Kalgutkar, A.S., Driscoll, J., Zhao, S.X., Walker, G.S., Shepard, R.M., Soglia, J.R., Atherton, J., Yu, L., Mutlib, A.E., Munchhof, M.J., Reiter, L.A., Jones, C.S., Doty, J.L., Trevena, K.A., Shaffer, C.L., Ripp, S.L., 2007. Bioactivation liabilities associated with a nonpeptidyl thrombopoietin receptor agonist containing a 2-amino-4-arylthiazole motif. Chem. Res. Toxicol. 20, 1954–1965.

Kleinpeter, E., 2006. Push-pull alkenes: structure and pi-electron distribution. J. Serb. Chem. Soc 71, 1–17. https://doi.org/10.2298/JSC0601001K.

Kumar, S., Patil, M.T., Kataria, R., Salnuke, D.B., 2016. Thiazole: a privileged scaffold in drug discovery. Chemical Drug Design.

Liakoni, E., Bravo, A.E.R., Krahenbuhl, S., 2015. Hepatotoxicity of new oral anticoagulants (NOACs). Drug Saf. 38, 711–720. https://doi.org/10.1007/s40264-015-0317-5.

Lin, Y., Lu, P., Tang, C., Mei, Q., Sandig, G., Rodrigues, A.D., Rushmore, T.H., Shou, M., 2001. Substrate inhibition kinetics for cytochrome P450-Catalyzed reactions. Drug Metab. Dispos. 29, 368–374.

LiverTox [WWW Document], 2018. U.S. National Library of Medicine, National Institutes of Health. URL https://livertox.nih.gov/. .

Matlock, M.K., Datta, A., Dang, N.L., Jiang, K., Swamidass, S.J., 2019. Deep learning long-range information in undirected graphs with wave networks. Proceedings of the International Joint Conference on Neural Networks.

Mizutani, T., Ito, K., Nomura, H., Nakanishi, K., 1990. Nephrotoxicity of thiabendazole in mice depleted of glutathione by treatment with DL-buthionine sulfoximine. Food Chem. Toxicol. 28, 169–177.

Mizutani, T., Yoshida, K., Ito, K., 1992. Nephrotoxicity of thiazoles strucutrally related to thiabendazole in mice depleted of glutathione by treatment with buthionine sulfoximine. Biochem. Biophys. Res. Commun.

Mizutani, T., Yoshida, K., Kawazoe, S., 1994a. Formation of toxic metabolites from thiabendazole and other thiazoles in mice: identification of thioamides as ring cleavage products. Drug Metab. Dispos. 22, 750–755.

Mizutani, T., Yoshida, K., Kawazoe, S., 1994b. Formation of toxic metabolites from thiabendazole and other thiazoles in mice: identification of thioamides as ring cleavage products. Drug Metab. Dispos. 22, 750–755.

Morisseau, C., Newman, J.W., Dowdy, D.L., Goodrow, M.H., Hammock, B.D., 2001. Inhibition of microsomal epoxide hydrolases by Ureas, amides, and amines. Chem. Res. Toxicol. 14, 409–415. https://doi.org/10.1021/tx0001732.

Neal, R.A., Halpert, J., 1982. Toxicology of thiono-sulfur compounds. Annu. Rev. Pharmacol. Toxicol. 22, 321–339.

Niwa, T., Murayama, N., Tamazaki, H., 2008. Heterotropic cooperativity in oxidation mediated by cytochrome P450. Curr. Drug Metab. 9, 453–462.

Obach, R.S., Kalgutkar, A.S., Ryder, T.F., Walker, G.S., 2008. In vitro metabolism and covalent binding of enol-carboxamide derivatives and anti-inflammatory agents sudoxicam and meloxicam : insights into the hepatotoxicity of Sudoxicam. Chem. Res. Toxicol. 1890–1899.

Ogasawara, Y., Tanaka, R., Koike, S., Horiuchi, Y., Miyashita, M., Arai, M., 2016. Determination of methylglyoxal in human blood plasma using fluorescence high performance liquid chromatography after. J. Chromatogr. B 1030, 102–105.

Reliant, 2004. Axid (nizatidine) Oral Solution. U. S. Food and Drug Administration.

Rostom, A., Goldkind, L., Laine, L., 2005. Nonsteroidal anti-inflammatory drugs and hepatic toxicity: a systematic review of randomized controlled trials in arthritis patients. Clin. Gastroenterol. Hepatol. 3, 489–498.

Sasaki, K., Lahoti, A., Jabbour, E., Jain, P., Pierce, S., Borthakur, G., Daver, N., Kadia, T., Pemmaraju, N., Ferrajoli, A., O'Brien, S., Kantarjian, H., Cortes, J., 2016. Clinical safety and efficacy of nilotinib or dasatinib in patients with newly diagnosed chronic-phase chronic myelogenous leukemia and pre-existing liver and/or renal dysfunction. Clin. Lymphoma Myeloma Leuk. 16, 152–162. https://doi.org/10.1016/j.clml.2015.12.003.Clinical.

Schmid, J., Busch, U., Heinzel, G., Bozler, G., Kaschke, S., Kummer, M., 1995. MELOXICAM pharmacokinetics and metabolic pattern after intravenous subjects

infusion and oral administration to healthy accepted. Drug Metab. Dispos. 23, 1206–1213.
Smith, G.F., 2011. Designing drugs to avoid toxicity. Prog. Med. Chem. 50, 1–47. https://doi.org/10.1016/B978-0-12-381290-2.00001-X.
Staerkel, P., Horsmans, Y., 1999. Meloxicam-induced liver toxicity. Acta Gastroenterol. Belg. 62, 255–256.
Stigliani, J.-L., Bernardes-Genisson, V., 2019. New insights into the chemical behavior of S-oxide derivatives of thiocarbonyl-containing antitubercular drugs and the influence on their mechanism of action and toxicity. Ann. Pharm. Fr. 77, 126–135. https://doi.org/10.1016/j.pharma.2018.11.004.
Sulfathiazole [WWW Document], 2018. DrugBank. URL https://www.drugbank.ca/drugs/DB06147. .
Testa, B., Pedretti, A., Vistoli, G., 2012. Foundation review : reactions and enzymes in the metabolism of drugs and other xenobiotics. Drug Discov. Today 17, 549–560. https://doi.org/10.1016/j.drudis.2012.01.017.
Wiseman, E.H., Chiaini, J., 1972. Anti-inflammatory and pharmacokinetic properties of sudoxicam N-(2-thiazolyl)-4-hydroxy-2-methyl-2H-1,2-benzothiazine-3-carboxamide 1,1-dioxide. Biochem. Pharmacol. 21, 2323–2334. https://doi.org/10.1016/0006-2952(72)90383-8.
Yocum, D., Fleischmann, R., Dalgin, P., Caldwell, J., Hall, D., Roszko, P., 2000. Safety and efficacy of meloxicam in the treatment of osteoarthritis: a 12-Week, double-blind, multiple-dose, placebo-controlled trial. Arch. Intern. Med. 160, 2947–2954. https://doi.org/10.1001/archinte.160.19.2947.
Zhu, C., Byrd, R.H., Lu, P., Nocedal, J., 1997. Algorithm 778: L-BFGS-B: fortran subroutines for large-scale bound-constrained optimization. Acm Trans. Math. Softw. 23, 550–560. https://doi.org/10.1145/279232.279236.